Editors' Suggestion

Experimental demonstration of beam-driven wakefield acceleration in laser-plasma filament

M. Galletti,[1,*] L. Verra,[1] A. Biagioni,[1] M. Carillo,[1] L. Crincoli,[1] R. Demitra,[1] G. Di Pirro,[1] G. Parise,[1] R. Pompili,[1] F. Stocchi,[1,2] F. Villa,[1] A. Zigler,[3] and M. Ferrario[1]

[1]*INFN Laboratori Nazionali di Frascati, Via Enrico Fermi 54, 00044 Frascati, Italy*

[2]*Università di Roma Tor Vergata, Department of Physics, Via della Ricerca Scientifica 1, 00133 Rome, Italy*

[3]*Racah Institute of Physics, Hebrew University, Jerusalem 91904, Israel*

(Received 26 May 2026; accepted 29 September 2026; published 2 November 2026)

Self-guided femtosecond laser pulses propagating in low-pressure gas can generate plasma filaments, establishing a framework for plasma wakefield acceleration (PWFA). This method exploits the intrinsic nonlinear light-matter interaction, reducing the energy required to generate plasma while enabling the realization of plasma stages suitable for PWFA. Here we report a proof-of-principle experimental demonstration of beam-driven wakefield acceleration of electron bunches with an accelerating field exceeding 250 MV/m in a laser-generated plasma filament. The witness bunch is accelerated while preserving both its charge and relative energy spread. The robustness and reproducibility of both the plasma source and the acceleration process are demonstrated with successful witness acceleration observed in 95% of the events and an rms energy jitter below 0.5%. The experimental observations are in agreement with particle-in-cell simulations, providing a consistent description of the underlying physical processes. These results demonstrate that laser-generated plasma filaments can serve as reliable plasma stages, delivering beam quality and operational reproducibility comparable to those achieved with established plasma-generation techniques. The concept bridges laser filamentation physics and compact accelerator technologies, offering a promising route toward sustainable, high-repetition-rate plasma-based facilities.

DOI: 10.1103/qjd9-p6dy

I. INTRODUCTION

The propagation of ultrashort, high-intensity laser pulses in gases is governed by a dynamic balance between self-focusing and defocusing due to low-density plasma generated via multiphoton or tunnel ionization [1,2]. This balance leads to intensity clamping [3,4] and to the formation of extended plasma channels [5,6], commonly referred to as filaments. Under suitable conditions, filaments can extend over tens of meters [7,8] and have been observed over distances approaching two kilometers in atmospheric propagation [9].

Among numerous applications [10–12], the adoption of laser-plasma filaments as stages for plasma wakefield acceleration (PWFA [13]) represents another potential direction. When a charged particle bunch (the driver) travels in plasma, the plasma electrons move to shield the electromagnetic fields of the bunch [14], resulting in a plasma electron density oscillation behind the bunch. The plasma density wake sustains longitudinal and transverse wakefields [15] that can be used to accelerate a trailing bunch (the witness) to high energies over short distances [16,17], with quality suitable for applications such as radiation generation [18–20].

Conventionally, plasma stages for PWFA are generated by ionizing gas using high-current discharge capillaries [21–25], field ionization induced by relativistic charged-particle bunches [26], or laser-driven optical-field ionization techniques [27–35]. The latter include hydrodynamic optical-field-ionized (HOFI) plasma channels generated using quasi-Bessel beams, which have demonstrated efficient plasma-channel formation and compatibility with high-repetition-rate operation [31–35].

These techniques have enabled remarkable progress in plasma-based acceleration, including stable operation, low plasma density jitter, preservation of beam quality, and high-efficiency acceleration [22,24,36]. Nevertheless, they generally rely on dedicated discharge (high-voltage) circuits, high-energy laser systems, or tailored laser beam-shaping optics to generate and control the plasma stage.

In this paper, we present an alternative approach exploiting the intrinsic nonlinear propagation of an ultrashort laser pulse, leading to the formation of a self-guided plasma filament, eliminating the need for external dedicated subsystems or beam-shaping optics. The reduced deposited energy is distributed over the filament volume, reducing the thermal load per unit length and thereby offering a promising route toward high-repetition-rate operation. Moreover, the plasma filament transverse dimensions and length can be adjusted by varying the laser and gas parameters [37], and, in principle, the latter can be scaled to significantly longer interaction lengths through optimization of the propagation conditions.

We report a proof-of-principle experimental demonstration of the use of laser-plasma filaments as plasma stages

*Contact author: mario.galletti@lnf.infn.it

Published by the American Physical Society under the terms of the Creative Commons Attribution 4.0 International license. Further distribution of this work must maintain attribution to the author(s) and the published article's title, journal citation, and DOI.

for PWFA, achieving high-gradient acceleration exceeding 250 MV/m. The witness bunch is accelerated while preserving both its charge and relative energy spread. The robustness and reproducibility of both the plasma source and the acceleration process are demonstrated over 100 consecutive shots, with successful witness acceleration observed in ∼95% of the events and an rms energy jitter below 0.5%.

The plasma evolution is characterized through the analysis of the recombination light and is benchmarked against particle-in-cell simulations, showing excellent agreement and providing a consistent description of the underlying physical processes.

Beyond demonstrating an alternative plasma-generation scheme, this work establishes filament-generated plasmas as a viable and reliable platform for beam-driven plasma wakefield acceleration, bridging laser filamentation physics and compact accelerator technologies, delivering beam quality and operational reproducibility comparable to those achieved with established plasma-generation techniques and offering a promising route toward sustainable, high-repetition-rate user plasma-based facilities.

II. FILAMENTATION PHYSICS

Filamentation of high-power femtosecond laser pulses involves [38] several nonlinear effects such as diffraction, self-focusing, and group-velocity dispersion, as well as plasma generation and energy losses due to multiphoton and tunnel ionization [39,40]. To investigate the phenomenon, we adopt a theoretical model based on the nonlinear wave equation using the slowly varying envelope approximation [39,41–44] describing the electric field $A \equiv A(x, y, z, t)$ as [37]

$$\frac{\partial A}{\partial z} = \frac{i}{2k}\left(\frac{\partial^2}{\partial x^2} + \frac{\partial^2}{\partial y^2}\right)A - \frac{ik''}{2}\frac{\partial^2}{\partial t^2}A + ik_0 n_2\left((1-f)I + f\int_{-\infty}^{t} R(t-t')I(t')dt'\right)A - \frac{\sigma}{2}(1+i\omega_0\tau_c)n_{pe}A - \frac{\beta_K}{2}I^{K-1}A, \quad (1)$$

where $I = |A(x, y, z, t)|^2$ is the intensity of the laser pulse, ω_0 and k the laser frequency and wave number. On the right-hand side, the first term accounts for diffraction within the transverse planes; the second term for the group velocity dispersion (GVD) of an ultrashort laser pulse, where k'' (in units of fs^2/cm) is the GVD coefficient; and the third for the Kerr effect [39,41–43,45,46]. A constant factor $k_0 n_2$, where $k_0 = \omega_0\tau_c/n_0$ (τ_c the characteristic time for electron-neutral inverse Bremsstrahlung, n_0 the linear index of refraction) and n_2 (in units of cm^2/W) is the nonlinear index of refraction, accounting for the nonlinear effects arising from the specific laser and gas parameters involved [47,48], is multiplied by the instantaneous and delayed Kerr components given in parentheses, where $f = 0.5$ is the coefficient due to stimulated molecular Raman scattering [39,49] and $R(t)$ is the exponential function with a characteristic time (τ_R) of about 70 fs; the fourth term for plasma absorption and defocusing where σ is the cross-section for the inverse Bremsstrahlung process following the Drude model [41,50], and $n_{pe} \equiv n_{pe}(x, y, z, t)$ the electron density of the plasma generated by ionization; finally,

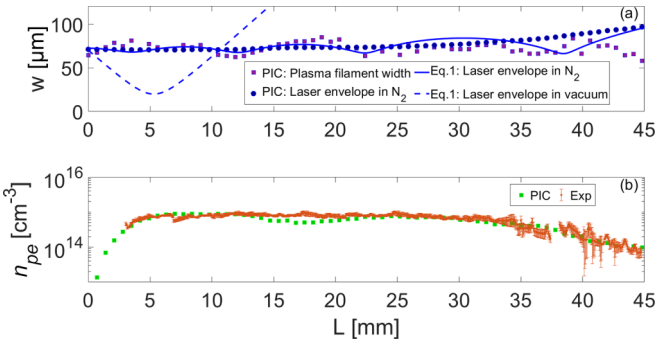


FIG. 1. Laser filamentation simulations. (a) Laser pulse nonlinear propagation retrieved via the envelope equation [Eq. (1)] in nitrogen gas (blue continuous line) and in vacuum (blue dashed line); laser pulse nonlinear propagation (blue circles) and plasma filament width (violet squares) retrieved from PIC simulation. (b) Longitudinal plasma density distribution retrieved from PIC simulations (green squares) and from transverse imaging of the filament (orange circles) as in the inset of Fig. 3.

the last term accounts for energy absorption due to ionization, where β_K is the multi-photon ionization rate parameter [43,51], and K the number of photons needed to ionize each atom or molecule once.

The solid blue line in Fig. 1 shows the transverse envelope of a laser pulse with central wavelength $\lambda = 800$ nm, root mean square (rms) transverse size at waist $w_0 = 20$ μm in vacuum (Rayleigh length $Z_R = \pi w_0^2/\lambda = 1.5$ mm) and full width half maximum (FWHM) duration $\tau = 350$ fs, interacting with neutral nitrogen gas with density $n_N = 10^{16}$ cm^{-3}, obtained solving Eq. (1). We consider a longitudinal density profile with a plateau from 5 to 35 mm and smooth ramps at the entrance and exit. Calculations show that, because of the occurrence of filamentation, the pulse is self-guided for ∼45 mm, corresponding to $\sim 30\, Z_R$, with an average transverse size $w_L \sim 70$ μm. The dashed blue line shows the corresponding envelope of the pulse when propagating in vacuum. When filamentation occurs, the focal plane is shifted upstream, and the waist is larger than when propagating in vacuum.

We compare the theoretical results with particle-in-cell (PIC) numerical simulation results obtained with FBPIC [52]. [1]

To capture the filamentation process self-consistently, we modified the PIC code to include the Kerr response as an additional polarization current in Ampère's law, alongside the free-electron plasma current. The nonlinear polarization is written as the sum of an instantaneous and a delayed term, as in Eq. (1),

$$P_{\mathrm{Kerr}}(t) = \varepsilon_0\chi^{(3)}A\left[(1-f)\,I + f\int R(t-t')\,I(t')\,dt'\right], \quad (2)$$

where ε_0 is the vacuum permittivity and $\chi^{(3)}$ is the third-order nonlinear susceptibility of the neutral gas, responsible for the Kerr effect, so that both Kerr contributions evolve self-consistently with the plasma.

[1] For the code documentation, see [53].

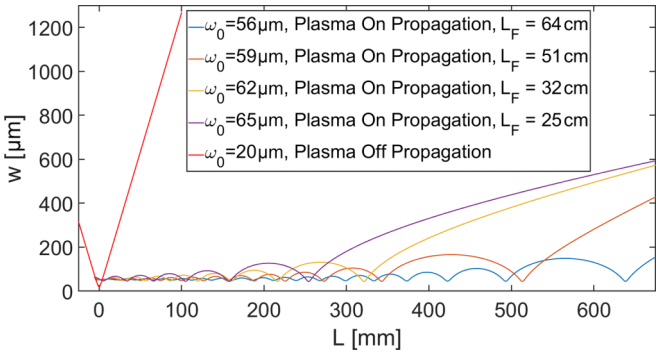


FIG. 2. Solution of the laser envelope equation for the same laser pulse energy and gas density used in the experiment, varying only the initial laser spot size. The red curve shows the corresponding vacuum propagation for a tightly focused Gaussian beam, illustrating the extension of the interaction length, enabled by the balance between Kerr self-focusing and plasma defocusing, through the transverse matching conditions without increasing the laser pulse energy.

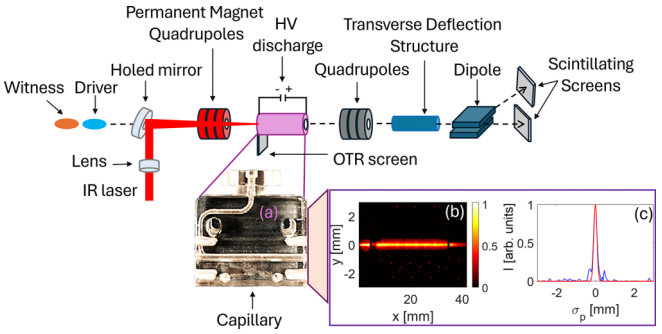


FIG. 3. Experimental setup. Schematic layout of the SPARC_LAB linac interaction chamber arranged for the plasma filament-based acceleration experimental campaign. (a) 45°, single-inlet capillary design. (b) Typical filament snapshots taken via the side imaging technique and (c) relative transverse profile (blue line) fitted with a Gaussian function with $\sigma = 70\,\mu$m (red line).

The Gaussian laser is initialized with the same parameters as those experimentally measured, and its evolution is computed using the OpenPMD library.[2] The laser interacts with a $\sim$ 3-cm-long column of neutral nitrogen gas of $n_N = 10^{16}\,\mathrm{cm}^{-3}$ adopting the longitudinal neutral density distribution retrieved from OpenFOAM simulations. Ionization is modeled using the Ammosov-Delone-Krainov theory [55].

The transverse size of the laser pulse, calculated from the laser electromagnetic fields (blue circles in Fig. 1), is in good agreement with the theoretical one. We also extract the width of the plasma channel w_{FIL} (purple squares in Fig. 1), calculating the rms of the transverse distribution of the plasma electron density of the filament after the pulse has passed. The width of the filament is $\sim$70 μm on average, and it oscillates between 60 μm and 85 μm, with a behavior similar to that of the laser pulse envelope. The on-axis plasma electron density obtained from the PIC simulations (n_{pe} PIC, green squares in Fig. 1) reaches an average value of $\sim 8 \times 10^{14}\,\mathrm{cm}^{-3}$, along the 3-cm-long plateau corresponding to that of the neutral gas density distribution.

The agreement between the experimental observations and the numerical description of the filament propagation provides confidence that the model can be employed to investigate the scalability of the proposed plasma source beyond the conditions accessible in the present experiment.

While the experimental campaign was performed for a single set of plasma parameters, corresponding to the interaction length required by the available PWFA setup, the filamentation process intrinsically offers a broad degree of flexibility. In particular, besides the plasma density, which can be adjusted through the gas pressure and laser pulse parameters [37], the interaction length can be controlled by properly matching the laser beam to the nonlinear propagation conditions.

To illustrate this capability, Fig. 2 reports the solution of the laser envelope equation for the same laser pulse energy and gas density adopted in the experiment, while varying only the initial transverse beam size. Despite identical laser energy and propagation medium, different transverse matching conditions produce stable self-guided propagation over substantially different distances, with filament length ranging from approximately 25 cm up to more than 60 cm. In contrast, the propagation of a Gaussian beam in vacuum (red curve) rapidly diverges after the focal plane and cannot sustain high intensity over comparable distances.

This behavior highlights one of the distinctive features of filamentation. The achievable plasma length is not limited by the diffraction-limited Rayleigh range of the incident laser beam, but is instead determined by the dynamic balance between Kerr self-focusing and plasma defocusing, which continuously replenishes the laser intensity and sustains the self-guided propagation. As a consequence, for a fixed laser pulse energy and gas density, the plasma length becomes a design parameter that can be tailored through the transverse matching conditions. These results suggest that filament-generated plasma stages may offer a promising route toward longer interaction lengths while preserving the low deposited energy and operational simplicity that make this approach attractive for future high-repetition-rate plasma wakefield accelerators.

III. EXPERIMENTAL SETUP

The experiment took place at the SPARC_LAB facility at the INFN-Frascati National Laboratory [56,57] (see Fig. 3). The SPARC_LAB bunker hosts a Ti:Sapphire chirped pulse amplification [58] laser system, which delivers 80 mJ laser pulses at 800 nm central wavelength, with a transform-limited duration of 30 fs at FWHM, and a repetition rate of 10 Hz. The output of the laser system [19,57,59] is split into two beamlines.

In the first one (linac beamline), the pulse is frequency-doubled to generate electron (e^-) bunches illuminating a copper cathode within a radio frequency (rf) gun. Multiple bunches in the same rf bucket can be generated by splitting and delaying the main pulse in replicas with adjustable delay and relative intensity [59,60]. The bunches are then

[2]For documentation, see [54].

accelerated ($E \sim 97$ MeV) and longitudinally compressed (subpicosecond) via velocity-bunching [61,62] in the rf linac, and transversally focused with a triplet of permanent magnet quadrupoles at the entrance of a 2-mm-diameter, 3-cm-long, single-inlet dielectric capillary.

The second beamline (filament beamline) delivers pulses with ∼10 mJ (∼0.7% energy jitter), 350 fs (FWHM), and transverse size ∼25 mm at $1/e^2$ intensity at a 2″ 1-m-focal-length lens location, focusing the pulse at the entrance of the capillary, after being reflected by a 45° holed mirror through which the electron bunches propagate.

We measure the time of arrival of the electron bunches with respect to the peak of the IR laser pulse with the analog signal generated by a beam position monitor upstream of the vacuum chamber with a GHz scope. The timing jitter between the bunch and the IR laser is negligible, being generated by the same main laser system. As a result, the plasma density at the electron bunches' arrival time is constant from event to event. By varying the delay between the laser pulse and the electron bunches' arrival time, we vary n_{pe} due to recombination of the plasma. The laser pulse reaches the capillary entrance approximately 100 ps before the arrival of the electron bunches to optimize the acceleration process.

The capillary, shown in Fig. 3(a), is filled with nitrogen gas through a solenoid valve 1.5 ms before the arrival of the laser pulse, and plasma is generated by filamentation. The inset of Fig. 3(b) shows the plasma filament obtained by imaging the recombination light of the plasma onto a multichannel plate coupled to a CCD camera (side imaging technique). From these snapshots, we calculate the length of about 45 mm (full width at tenth maximum) and rms transverse size around 70 μm. The black regions along the filament are due to the metallic electrodes installed on the capillary for the ionization with the high-current discharge.

We obtain the longitudinal density profile of the plasma by projecting the pixel counts along the vertical axis. The intensity of the plasma-emitted light is directly related, through the Einstein coefficient, to the number of ions in the excited state, which, up to a calibration factor, provides a measure of the plasma density [6,63]. To determine the plasma density, the emitted light intensity is calibrated using the Stark broadening technique. The trend of the resulting intensity profile (orange dots in Fig. 1) is in good agreement with the longitudinal plasma density profile obtained by numerical simulations. Since the intensity of the light is correlated with the plasma density, we estimate a density jitter of 6.8% in the plateau region (5–35 mm, shown in Fig. 1).

The larger jitter observed in the integrated plasma filament signal (∼6.8%), compared with the laser energy jitter (∼0.7%), likely arises from the combined fluctuations in pulse's energy and spatiotemporal profile, and in gas-target properties (density distribution, flow, turbulence).

We measure the position and transverse distribution of the electron bunches and of the attenuated laser pulse at the capillary entrance using an aluminated silicon screen. The screen is installed below the entrance of the capillary, and it is inserted in the beam path by moving the capillary vertically with a step motor. The optical transition radiation (OTR) emitted by the electrons or the reflected laser pulse is imaged onto the chip of a digital camera.

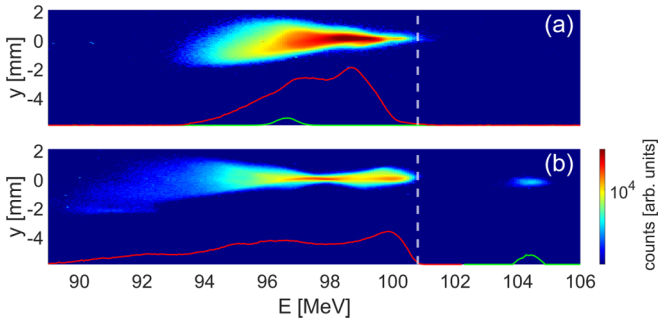


FIG. 4. Experimental energy spectra. Energy spectrum of driver and witness bunches in the (a) laser-off and (b) laser-on configurations, while gas is present in the capillary. The color bar is the same for both panels. The color scale is linear. Solid lines: Energy distribution of driver (red) and witness (green).

We characterize the electron bunches' energy and longitudinal distribution using a magnetic spectrometer composed of a triplet of electromagnetic quadrupoles, a transverse deflection structure [64] (introducing a head-to-tail vertical correlation to the bunch), a magnetic dipole (dispersing the beam in the horizontal plane), and a scintillating screen.

The rms duration of the driver and witness bunches (obtained by calculating the rms of the longitudinal bunch distribution on the screen with TDS turned on) is $\sigma_t = (0.6, 0.2) \pm 0.1$ ps, respectively. The temporal distance between the two bunches is $\Delta t = 2.7 \pm 0.1$ ps. We calculate the bunch density $n_b = (Q/q)/(2\pi)^{3/2} c\sigma_t \sigma_r^2$, where Q is the charge per bunch and σ_r is the rms transverse size at the plasma entrance (measured with the OTR screen). The bunches have $Q = (500, 50) \pm 1$ pC, and $\sigma_r = (27, 20) \pm 3$ μm, thus $n_b = (1.5, 0.82) \times 10^{15}$ cm^{-3}. Hence, we expect the driver bunch to generate wakefields in the blowout regime ($n_b \gg n_{pe} = 8 \times 10^{14}$ cm^{-3}) and the witness bunch to be placed in the accelerating and focusing phase of the wakefields. The normalized emittance of the bunches is ∼2.9 μm (measured with a quadrupole scan technique).

IV. EXPERIMENTAL RESULTS

Figure 4 shows the energy spectra of driver and witness bunches averaged over 100 consecutive events after propagation through the gas-filled capillary without (a) and with (b) the ionizing laser pulse. The red and green projections on the energy axis show the energy distribution of the driver and witness bunch, respectively. By comparing the spectra, we retrieve a maximum deceleration of the driver[3] $\Delta E_D^- \sim 4$ MeV and an average acceleration of the witness $\Delta E_W^+ \sim 8$ MeV, reaching a final energy $E_W = 104.5 \pm 0.4$ MeV, when the laser pulse is present. This is due to the fact that the laser pulse interacts with the gas, generating the plasma filament within

[3]We define the minimum and maximum energy of each bunch as the values where the amplitude of the energy distribution reaches 10% of its own maximum on the low and high-energy sides, while the mean energy is the centroid of the spectral distribution.

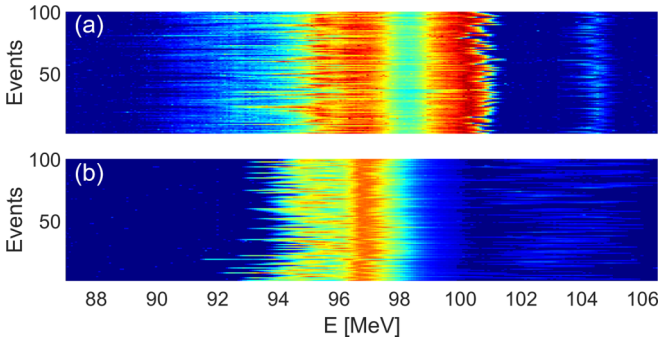


FIG. 5. Waterfall plot of experimental energy distributions. Energy distribution of driver and witness bunches of 100 consecutive events in the (a) laser-on and (b) discharge-on configuration, while gas is present in the capillary with similar initial beam parameters and the same average plasma electron density. The intensity of each plot is normalised with respect to the maximum of (a). The color scale in both panels is linear.

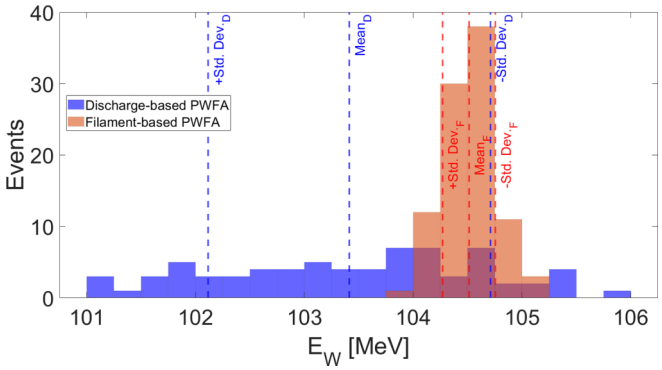


FIG. 6. Comparison between the filament-based PWFA and the discharge-based PWFA. Histogram of the accelerated witness energy E_W in both filament-based (orange area) and discharge-based (blue area) configurations.

which the electron bunch drives the wakefields. Considering a 3-cm-long plasma, the average accelerating gradient is $E_z^+ \sim 266\,\mathrm{MeV/m}$. We note that the charge and the relative energy spread of the witness bunch are preserved upon acceleration.

The robustness and reproducibility of the plasma filament generation and of the acceleration process are clearly evidenced by Fig. 5(a), where we show the energy distribution of 100 consecutive events. The witness bunch is accelerated in 95% of the events, and the rms energy jitter is <0.5%, meaning a plasma stage with minimized density and timing jitter. Notably, the fact that the witness beam energy jitter remains well below 1% suggests that the filament core, relevant to the wakefield excitation, is more reproducible (<6.8%) than the integrated Intensified CCD (charge-coupled device) signal indicates; we plan future work to further characterize this aspect.

An additional demonstration of reliable and repeatable operation of the proposed setup is directly given by a direct comparison with the discharge-based plasma source without the stabilization subsystem, which is an established setup for PWFA [18–20].

These results demonstrate that a filament-generated plasma can sustain beam-driven wakefield acceleration with beam quality, operational reproducibility, and shot-to-shot stability comparable to state-of-the-art stabilized discharge plasma sources [22–25,36,65], maintaining a simple and compact setup.

Differently from conventional discharge-based plasma sources, which typically rely on high-voltage discharge systems, dedicated synchronization and stabilization subsystems, and supporting plasma-source structures such as sapphire/ceraminc capillary discharges [22,23,36,65] or water-cooled alumina capillaries for long-term high-repetition-rate operation [24,25], the present approach requires only a gas target (3D-printed plastic capillary) and a low-energy ultrashort laser pulse to generate the plasma stage.

Furthermore, it should be noted that in this setup, the capillary serves solely as a gas containment cell, so its diameter could be increased or completely removed. The only constraint is given by the beamline pumping system, which could be upgraded to zero the wall load.

Figure 5(b) shows that the witness bunch is accelerated in a discharge-based plasma (7 kV, 233 A, preserving the plasma stage structure and without additional stabilization methods [66,67]) in only 75% of the events, with rms energy jitter of ∼1.3%, meaning a threefold increase with respect to the filament configuration, with a comparable energy gain but a relative energy spread of approximately 4%. This is due to the fact that in the discharge configuration, the ionization process is initiated in a stochastic manner, affecting the plasma density and therefore the acceleration process.

We calculate the average energy of the witness bunch E_W of each successful acceleration event. The corresponding histograms in Fig. 6 clearly show that the energy variation in the filament case (orange area) is much smaller than in the discharge case (blue area). This is due to the higher reproducibility and inherent synchronization of the system with the rf linac.

V. DISCUSSION

In the present work, we conducted a proof-of-principle experiment to demonstrate the use of laser filamentation for the generation of plasma stages suitable for PWFA. To obtain further insights into the plasma properties, we compare the experimental results with numerical PIC simulations. The plasma is initialized with a transverse Gaussian distribution with rms $\sigma_p = 70\,\mu\mathrm{m}$ and on-axis $n_{pe} = 8 \times 10^{14}\,\mathrm{cm}^{-3}$. Figure 7 shows the longitudinal (solid blue line) and transverse (dashed blue line) wakefields driven by an e^- bunch with the same parameters as those experimentally measured (driver and witness charge density distributions shown by the red and green lines, respectively, centered at $t = 0$, traveling from left to right). The plasma density distribution and the properties of the wakefields behind the driver bunch ($t < 0$) are those typical of the blowout regime, as expected by $n_b \gg n_{pe}$.

The amplitude of the decelerating wakefields within the driver bunch reaches ∼150 MV/m, while that of the accelerating wakefields within the witness bunch ($t = -2.7\,\mathrm{ps}$) reaches ∼260 MV/m. Considering a 3-cm long plasma, the amplitude of the longitudinal wakefields is in agreement with the energy loss and gain experimentally measured. Hence, we

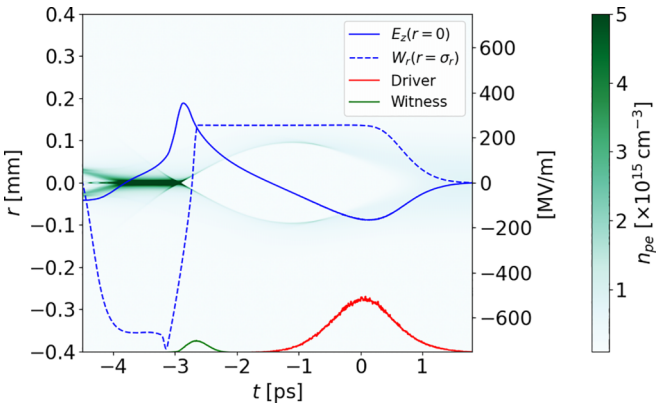


FIG. 7. PWFA PIC simulations. Color map: 2D plasma electron density distribution. Right-hand side axis: blue line, the on-axis ($r = 0$) longitudinal (E_z) wakefield; blue dashed line, the transverse (W_r) wakefields at $r = \sigma_r$. The charge density distribution of the driver bunch (red line) and of the witness bunch (green line) is shown in normalized units.

conclude that the interaction of the laser pulse with the gas generates plasma with a longitudinal profile consistent with the one shown in Fig. 1 and a transverse Gaussian profile with $\sigma_p = 70$ μm.

We have experimentally demonstrated the generation of an operational PWFA stage satisfying several essential requirements, including controlled plasma parameters and highly reproducible operation. The filamentation-based approach enables plasma formation with reduced generating system energy compared to conventional PWFA and LWFA plasma sources for comparable plasma lengths and densities.

In the configuration presented here, a commercial *GW*-class laser is sufficient to sustain the plasma channel, whereas alternative approaches require either TW-class laser systems for laser-ionized vapor sources [17,68,69], GeV-class relativistic electron beams as drivers in beam-driven plasma wakefield acceleration, or high-voltage discharge circuits for capillary-based plasma channels [22–25]. In discharge-based systems, plasma formation relies on gas breakdown and ohmic heating of the bulk medium, which generally requires substantially higher energy deposition compared to optical-field or filamentation-based ionization.

The filamentation-based configuration results in negligible thermal loading even at high repetition rates, owing to the low deposited energy and the absence of a solid confining structure, also because of the transverse size of the plasma column. In the experiment presented here, we measured an energy loss of ∼2.5 mJ per laser pulse (assuming conservatively that all the energy is deposited on the wall, even though most of this energy is actually lost in the beam transport through the recapturing permanent magnetic quadrupoles and vacuum impedance downstream of the capillary). For a 3-cm-long interaction region, this corresponds to an effective energy deposition well below typical damage thresholds.

In contrast, optimized discharge-capillary systems employ sapphire [22,23] or alumina (Al_2O_3) [24,25] capillaries filled with hydrogen, where energy deposition per shot can reach $\mathcal{O}(10^2)$ mJ in short stages and increase further in longer accelerator configurations [70,71].

In fact, in a separate experiment, we measured an energy deposition of approximately 100 mJ per discharge in a 3-cm-long capillary, increasing to about 2 J per discharge in a 60-cm-long capillary (as envisioned for the EuPRAXIA@SPARC_LAB project [70,71]). Such systems demonstrate excellent stability and performance, but require careful thermal management (as cooling systems or high thermal load material) and robust materials (high mechanical strength) to mitigate gradual degradation of the capillary surface [24,72]. Once the capillary channel is degraded through operation, the resulting plasma profile is altered, leading to a nonoptimized acceleration process.

The repetition rate in filamentation-based schemes is primarily limited by the laser system. Modern mJ-class femtosecond lasers can operate at kHz repetition rates, consistent with other laser-driven plasma channel and HOFI-based demonstrations [31–35]. HOFI channels, in particular, provide a related regime of laser-driven plasma formation without solid boundaries, with demonstrated scalability and kHz compatibility. In contrast, discharge-based capillary systems are typically limited by the high-voltage pulser and thermal load management, with stable operation routinely achieved at ∼100 Hz and only in specific configurations approaching higher repetition rates [24,25]. Beam-driven plasma wakefield acceleration in laser-ionized vapor plasmas (e.g., lithium and rubidium plasmas) [17,68,69] employing high-energy laser systems (Joule-class) is intrinsically limited to low repetition-rate operation. Within this landscape, filamentation-based plasma generation provides an additional pathway characterized by low energy requirements, intrinsic simplicity, and compatibility with high-repetition-rate operation.

An additional advantage of the proposed scheme is intrinsic synchronization between plasma generation and electron beams, since both are driven by the same laser system used for photocathode emission. In contrast, discharge-based plasma sources require an external high-voltage pulser unit, which must be actively synchronized with the accelerator timing system [23]. This additional layer of timing coordination can introduce jitter and reduce overall reproducibility. Discharge-based systems, where the breakdown process is initiated in a stochastic and uncontrolled manner, exhibit timing jitter that can be minimized by implementing an additional stabilisation system, as in Refs. [67,73].

The same issue is encountered in externally (not shared with the photocathode system) laser-based schemes for different laser-ionization-based approaches. HOFI channels [31–35] and laser-ionized vapour plasmas (e.g., lithium and rubidium systems used in Refs. [17,68,69]) require controlled ionization timing and, in some cases, more complex coordination between laser systems and beam drivers, increasing overall synchronization requirements.

From a scalability perspective, in filamentation-based PWFA stages, the plasma length and density can be flexibly tuned via laser parameters and gas conditions, as described by Eq. (1) and shown in Fig. 2. Unlike capillary-based systems [22], where geometry is fixed by the solid structure (typically sapphire or alumina capillaries of 3-15 cm in present experiments [23]), filamentation allows the formation of self-guided plasma channels without physical confinement. Laser-based plasma schemes [17,31–35,68,69] are ultimately constrained

not only by available laser energy but also by requirements on target control, focusing conditions, beam shaping, and nonlinear propagation control, which further impact scalability in practical accelerator configurations. While filamentation-based channels rely on self-organization of the laser pulse in the medium, extension to longer interaction lengths typically requires optimization of input energy, beam quality, and focusing geometry, as well as control of propagation dynamics in the nonlinear regime.

Finally, this technique enables the generation of plasma channels with adjustable transverse dimensions. For example, it is possible to obtain plasma channels much narrower than the driver bunch, enabling ion-channel applications [74], since all plasma electrons would be expelled from the plasma and are not able to restore their initial condition, as envisioned for future plasma-based undulators. Finite-width plasma stages may also be suitable for positron acceleration, thanks to the extended accelerating and (transversely linear) focusing region for positively charged particles [75] (see Fig. 7, $-4.4\,\mathrm{ps} < t < -4.0\,\mathrm{ps}$), which are required for next-generation plasma-based lepton collider [76].

VI. CONCLUSIONS

We have conducted a proof-of-principle experimental demonstration, supported by numerical simulations and theoretical analysis, showing that self-guided femtosecond laser pulses propagating in low-pressure gas can generate plasma filaments suitable for beam-driven plasma wakefield acceleration. This approach exploits the intrinsic nonlinear light–matter interaction of laser filamentation, enabling plasma formation with reduced energy requirements while providing tunable interaction stages.

The experiment demonstrates beam-driven wakefield acceleration of electron bunches in a laser-generated plasma filament, with accelerating fields exceeding $250\,\mathrm{MV/m}$. The witness beam is accelerated while preserving both its charge and relative energy spread. The robustness of the system is confirmed over 100 consecutive shots, with successful acceleration observed in $\sim$95% of the events and an rms energy jitter below 0.5%.

These results are in excellent agreement with particle-in-cell simulations, which reproduce the measured plasma evolution and confirm the underlying physical mechanism. Beyond performance, the filament-based approach provides a reproducible and stable plasma stage, demonstrating beam quality preservation and operational consistency comparable to established plasma-generation techniques. In addition, the low energy deposition on the gas environment and the absence of solid confinement suggest compatibility with high-repetition-rate operation, with potential scalability to longer interaction lengths and larger transverse dimensions.

These features, together with a simple and low-maintenance setup, make laser filamentation a promising candidate for future user plasma-based accelerators. In this context, the approach is directly aligned with the EuPRAXIA scientific case [71], which foresees high-repetition-rate operation of plasma stages with lengths of order 60 cm and densities around $10^{15}\,\mathrm{cm}^{-3}$, supporting GV/m-class accelerating fields while preserving the high brilliance of externally injected beams.

ACKNOWLEDGMENTS

This work has received funding from the European Union's Horizon Europe research and innovation program under Grant Agreement No. 101079773 (EuPRAXIA Preparatory Phase). We thank I. Balossino, M. Bellaveglia, F. Cardelli, C. Di Giulio, L. Piersanti, A. Vannozzi, A. Michelotti, F. Anelli, M. Ceccarelli, G. Grilli, M. Martini, G. Luminati, and L.A. Rossi for technical support; M. Del Giorno for maintenance and operation of the laser system; V. Lollo and M. Zottola for the experimental chamber installation; D. Pellegrini, G. Grilli, and T. De Nardis for the HV discharge pulser design, and all the machine operators involved in the experimental run. Technical support of the Department of Physics of Tor Vergata University of Rome, in particular, F. Bonaccorso for computational resource utilization support, is gratefully acknowledged.

M.G., R.P., and A.Z. conceived the experiment. M.G., R.P., L.V., and G.D.P planned and managed the experiment with input from all the coauthors. M.G., L.V., F.S., and F.V. managed the photo-cathode laser system and filament beamline. L.C., R.D., and A.B. designed and characterized the capillary system. M.G., M.C., R.D., A.B., F.S., L.V., and R.P. carried out the experimental campaign. M.G. and M.C. performed the data analysis. M.G., L.V., and G.P. provided numerical simulations. A.Z. and M.F. supervised the project. The manuscript was written by M.G. and L.V. with assistance from R.P. and A.Z. and input from all the coauthors. All authors extensively discussed the results and reviewed the manuscript.

DATA AVAILABILITY

There are no publicly available research data or software supporting this manuscript. Requests for further information or data should be sent to the authors.

[1] N. Aközbek, C. M. Bowden, and S. L. Chin, Propagation dynamics of ultra-short high-power laser pulses in air: Supercontinuum generation and transverse ring formation, J. Mod. Opt. **49**, 475 (2002).

[2] S. L. Chin, S. A. Hosseini, W. Liu, Q. Luo, F. Théberge, N. Aközbek, A. Becker, V. P. Kandidov, O. G. Kosareva, and H. Schroeder, The propagation of powerful femtosecond laser pulses in opticalmedia: Physics, applications, and new challenges, Can. J. Phys. **83**, 863 (2005).

[3] A. Becker, N. Aközbek, K. Vijayalakshmi, E. Oral, C. Bowden, and S. Chin, Intensity clamping and re-focusing of intense femtosecond laser pulses in nitrogen molecular gas, Appl. Phys. B **73**, 287 (2001).

[4] W. Liu, S. Petit, A. Becker, N. Aközbek, C. Bowden, and S. Chin, Intensity clamping of a femtosecond laser pulse in condensed matter, Opt. Commun. **202**, 189 (2002).

[5] J.-F. Gravel, Q. Luo, D. Boudreau, X. Tang, and S. Chin, Sensing of halocarbons using femtosecond laser-induced fluorescence, Anal. Chem. **76**, 4799 (2004).

[6] A. Talebpour, M. Abdel-Fattah, and S. Chin, Focusing limits of intense ultrafast laser pulses in a high pressure gas: Road to new spectroscopic source, Opt. Commun. **183**, 479 (2000).

[7] G. Méchain, C. D'Amico, Y.-B. André, S. Tzortzakis, M. Franco, B. Prade, A. Mysyrowicz, A. Couairon, E. Salmon, and R. Sauerbrey, Range of plasma filaments created in air by a multi-terawatt femtosecond laser, Opt. Commun. **247**, 171 (2005).

[8] J. Papeer, I. Dey, M. Botton, Z. Henis, A. D. Lad, M. Shaikh, D. Sarkar, K. Jana, S. Tata, S. L. Roy, Y. M. Ved, G. Ravindra Kumar, and A. Zigler, Towards remote lightning manipulation by meters-long plasma channels generated by ultra-short-pulse high-intensity lasers, Sci. Rep. **9**, 407 (2019).

[9] M. Rodriguez, R. Bourayou, G. Méjean, J. Kasparian, J. Yu, E. Salmon, A. Scholz, B. Stecklum, J. Eislöffel, U. Laux, A. P. Hatzes, R. Sauerbrey, L. Wöste, and J.-P. Wolf, Kilometer-range nonlinear propagation of femtosecond laser pulses, Phys. Rev. E **69**, 036607 (2004).

[10] H. Xu, W. Liu, and S. Chin, Remote time-resolved filament-induced breakdown spectroscopy of biological materials, Opt. Lett. **31**, 1540 (2006).

[11] J. Kasparian, M. Rodriguez, G. Méjean, J. Yu, E. Salmon, H. Wille, R. Bourayou, S. Frey, Y.-B. André, A. Mysyrowicz, R. Sauerbrey, J.-P. Wolf, and L. Wöste, White-light filaments for atmospheric analysis, Science **301**, 61 (2003).

[12] L. Bergé, S. Skupin, C. Köhler, I. Babushkin, and J. Herrmann, 3D numerical simulations of THz generation by two-color laser filaments, Phys. Rev. Lett. **110**, 073901 (2013).

[13] T. Tajima and J. M. Dawson, Laser electron accelerator, Phys. Rev. Lett. **43**, 267 (1979).

[14] L. Verra, M. Galletti, R. Pompili, A. Biagioni, M. Carillo, A. Cianchi, L. Crincoli, A. Curcio, F. Demurtas, G. Di Pirro, V. Lollo, G. Parise, D. Pellegrini, S. Romeo, G. J. Silvi, F. Villa, and M. Ferrario, Experimental observation of space-charge field screening of a relativistic particle bunch in plasma, Phys. Rev. Lett. **133**, 035001 (2024).

[15] P. Chen, J. M. Dawson, R. W. Huff, and T. Katsouleas, Acceleration of electrons by the interaction of a bunched electron beam with a plasma, Phys. Rev. Lett. **54**, 693 (1985).

[16] E. Kallos, T. Katsouleas, W. D. Kimura, K. Kusche, P. Muggli, I. Pavlishin, I. Pogorelsky, D. Stolyarov, and V. Yakimenko, High-gradient plasma-wakefield acceleration with two sub-picosecond electron bunches, Phys. Rev. Lett. **100**, 074802 (2008).

[17] M. Litos, E. Adli, W. An, C. I. Clarke, C. E. Clayton, S. Corde, J. P. Delahaye, R. J. England, A. S. Fisher, J. Frederico, S. Gessner, S. Z. Green, M. J. Hogan, C. Joshi, W. Lu, K. A. Marsh, W. B. Mori, P. Muggli, N. Vafaei-Najafabadi, D. Walz, *et al.*, High-efficiency acceleration of an electron beam in a plasma wakefield accelerator, Nature (London) **515**, 92 (2014).

[18] R. Pompili, D. Alesini, M. P. Anania, S. Arjmand, M. Behtouei, M. Bellaveglia, A. Biagioni, B. Buonomo, F. Cardelli, M. Carpanese, E. Chiadroni, A. Cianchi, G. Costa, A. Del Dotto, M. Del Giorno, F. Dipace, A. Doria, F. Filippi, M. Galletti, L. Giannessi, *et al.*, Free-electron lasing with compact beam-driven plasma wakefield accelerator, Nature (London) **605**, 659 (2022).

[19] M. Galletti, D. Alesini, M. P. Anania, S. Arjmand, M. Behtouei, M. Bellaveglia, A. Biagioni, B. Buonomo, F. Cardelli, M. Carpanese, E. Chiadroni, A. Cianchi, G. Costa, A. Del Dotto, M. Del Giorno, F. Dipace, A. Doria, F. Filippi, G. Franzini, L. Giannessi, *et al.*, Stable operation of a free-electron laser driven by a plasma accelerator, Phys. Rev. Lett. **129**, 234801 (2022).

[20] M. Galletti, R. Assmann, M. E. Couprie, M. Ferrario, L. Giannessi, A. Irman, R. Pompili, and W. Wang, Prospects for free-electron lasers powered by plasma-wakefield-accelerated beams, Nat. Photon. **18**, 780 (2024).

[21] W. P. Leemans, B. Nagler, A. J. Gonsalves, C. Tóth, K. Nakamura, C. G. R. Geddes, E. Esarey, C. B. Schroeder, and S. M. Hooker, GeV electron beams from a centimetre-scale accelerator, Nat. Phys. **2**, 696 (2006).

[22] G. Loisch, J. Engel, M. Gross, M. Hochberg, H. Huck, G. Koss, O. Lishilin, A. Oppelt, S. Philipp, D. Richter, F. Stephan, and P. Weidemann, Jitter mitigation in low density discharge plasma cells for wakefield accelerators, J. Appl. Phys. **125**, 063301 (2019).

[23] J. Wood *et al.*, Progress towards high-quality, high-repetition-rate plasma acceleration at flashforward, in *Proceedings of the IPAC24, 15th International Particle Accelerator Conference No. 15* (JACoW Publishing, Geneva, Switzerland, 2024), pp. 541–544.

[24] M. Turner, A. J. Gonsalves, S. S. Bulanov, C. Benedetti, N. A. Bobrova, V. A. Gasilov, P. V. Sasorov, G. Korn, K. Nakamura, J. van Tilborg, C. G. Geddes, C. B. Schroeder, and E. Esarey, Radial density profile and stability of capillary discharge plasma waveguides of lengths up to 40 cm, High Power Laser Sci. Eng. **9**, e17 (2021).

[25] A. J. Gonsalves, F. Liu, N. A. Bobrova, P. V. Sasorov, C. Pieronek, J. Daniels, S. Antipov, J. E. Butler, S. S. Bulanov, W. L. Waldron, D. E. Mittelberger, and W. P. Leemans, Demonstration of a high repetition rate capillary discharge waveguide, J. Appl. Phys. **119**, 033302 (2016).

[26] C. L. O'Connell, C. D. Barnes, F.-J. Decker, M. J. Hogan, R. Iverson, P. Krejcik, R. Siemann, D. R. Walz, C. E. Clayton, C. Huang, D. K. Johnson, C. Joshi, W. Lu, K. A. Marsh, W. Mori, M. Zhou, S. Deng, T. Katsouleas, P. Muggli, and E. Oz, Plasma production via field ionization, Phys. Rev. ST Accel. Beams **9**, 101301 (2006).

[27] P. Muggli, B. E. Blue, C. E. Clayton, S. Deng, F.-J. Decker, M. J. Hogan, C. Huang, R. Iverson, C. Joshi, T. C. Katsouleas, S. Lee, W. Lu, K. A. Marsh, W. B. Mori, C. L. O'Connell, P. Raimondi, R. Siemann, and D. Walz, Meter-scale plasma-wakefield accelerator driven by a matched electron beam, Phys. Rev. Lett. **93**, 014802 (2004).

[28] G. Demeter, J. T. Moody, M. A. Kedves, B. Ráczkevi, M. Aladi, A.-M. Bachmann, F. Batsch, F. Braunmüller, G. P. Djotyan, V. Fedosseev, F. Friebel, S. Gessner, E. Granados, E. Guran, M. Hüther, V. Lee, M. Martyanov, P. Muggli, E. Öz, H. Panuganti, *et al.*, Long-range propagation of ultrafast ionizing laser pulses in a resonant nonlinear medium, Phys. Rev. A **104**, 033506 (2021).

[29] B. Miao, J. E. Shrock, L. Feder, R. C. Hollinger, J. Morrison, R. Nedbailo, A. Picksley, H. Song, S. Wang, J. J. Rocca, and

H. M. Milchberg, Multi-GeV electron bunches from an all-optical laser wakefield accelerator, Phys. Rev. X **12**, 031038 (2022).

[30] K. Oubrerie, A. Leblanc, O. Kononenko, R. Lahaye, I. A. Andriyash, J. Gautier, J.-P. Goddet, L. Martelli, A. Tafzi, K. Ta Phuoc, *et al.*, Controlled acceleration of GeV electron beams in an all-optical plasma waveguide, Light Sci. Appl. **11**, 180 (2022).

[31] R. J. Shalloo, C. Arran, L. Corner, J. Holloway, J. Jonnerby, R. Walczak, H. M. Milchberg, and S. M. Hooker, Hydrodynamic optical-field-ionized plasma channels, Phys. Rev. E **97**, 053203 (2018).

[32] A. Picksley, A. Alejo, R. J. Shalloo, C. Arran, A. von Boetticher, L. Corner, J. A. Holloway, J. Jonnerby, O. Jakobsson, C. Thornton, R. Walczak, and S. M. Hooker, Meter-scale conditioned hydrodynamic optical-field-ionized plasma channels, Phys. Rev. E **102**, 053201 (2020).

[33] J. M. Garland, G. Tauscher, S. Bohlen, G. J. Boyle, R. D'Arcy, L. Goldberg, K. Põder, L. Schaper, B. Schmidt, and J. Osterhoff, Combining laser interferometry and plasma spectroscopy for spatially resolved high-sensitivity plasma density measurements in discharge capillaries, Rev. Sci. Instrum. **92**, 013505 (2021).

[34] V. Lee, R. Ariniello, D. Storey, S. Corde, C. Emma, S. Gessner, M. Hogan, A. Knetsch, N. Majernik, B. O'Shea, I. Rajkovic, and M. Litos, Precision alignment and tolerance of a plasma wakefield accelerator in a laser-ionized plasma source, Phys. Rev. Accel. Beams **29**, 041001 (2026).

[35] A. Alejo, J. Cowley, A. Picksley, R. Walczak, and S. M. Hooker, Demonstration of kilohertz operation of hydrodynamic optical-field-ionized plasma channels, Phys. Rev. Accel. Beams **25**, 011301 (2022).

[36] C. A. Lindstrøm, J. M. Garland, S. Schröder, L. Boulton, G. Boyle, J. Chappell, R. D'Arcy, P. Gonzalez, A. Knetsch, V. Libov, G. Loisch, A. Martinez de la Ossa, P. Niknejadi, K. Põder, L. Schaper, B. Schmidt, B. Sheeran, S. Wesch, J. Wood, and J. Osterhoff, Energy-spread preservation and high efficiency in a plasma-wakefield accelerator, Phys. Rev. Lett. **126**, 014801 (2021).

[37] M. Galletti, L. Crincoli, R. Pompili, L. Verra, F. Villa, R. Demitra, A. Biagioni, A. Zigler, and M. Ferrario, Femtosecond laser-induced plasma filaments for beam-driven plasma wakefield acceleration, Phys. Rev. E **111**, 025202 (2025).

[38] H. M. Milchberg, Y.-H. Chen, Y.-H. Cheng, N. Jhajj, J. P. Palastro, E. W. Rosenthal, S. Varma, J. K. Wahlstrand, and S. Zahedpour, The extreme nonlinear optics of gases and femtosecond optical filamentation, Phys. Plasmas **21**, 100901 (2014).

[39] A. Couairon, Light bullets from femtosecond filamentation, Eur. Phys. J. D **27**, 159 (2003).

[40] N. L. Aleksandrov, S. B. Bodrov, M. V. Tsarev, A. A. Murzanev, Y. A. Sergeev, Y. A. Malkov, and A. N. Stepanov, Decay of femtosecond laser-induced plasma filaments in air, nitrogen, and argon for atmospheric and subatmospheric pressures, Phys. Rev. E **94**, 013204 (2016).

[41] A. Couairon, Filamentation length of powerful laser pulses, Appl. Phys. B **76**, 789 (2003).

[42] M. Mlejnek, E. Wright, and J. Moloney, Dynamic spatial replenishment of femtosecond pulses propagating in air, Opt. Lett. **23**, 382 (1998).

[43] V. P. Kandidov, O. G. Kosareva, I. S. Golubtsov, W. Liu, A. Becker, N. Akozbek, C. M. Bowden, and S. L. Chin, Self-transformation of a powerful femtosecond laser pulse into a white-light laser pulse in bulk optical media (or supercontinuum generation), Appl. Phys. B **77**, 149 (2003).

[44] N. Aközbek, M. Scalora, C. M. Bowden, and S. L. Chin, White-light continuum generation and filamentation during the propagation of ultra-short laser pulses in air, Opt. Commun. **191**, 353 (2001).

[45] P. Sprangle, J. R. Peñano, and B. Hafizi, Propagation of intense short laser pulses in the atmosphere, Phys. Rev. E **66**, 046418 (2002).

[46] P. Sprangle, J. R. Peñano, B. Hafizi, and C. A. Kapetanakos, Ultrashort laser pulses and electromagnetic pulse generation in air and on dielectric surfaces, Phys. Rev. E **69**, 066415 (2004).

[47] Á. Börzsönyi, Z. Heiner, A. P. Kovács, M. P. Kalashnikov, and K. Osvay, Measurement of pressure dependent nonlinear refractive index of inert gases, Opt. Express **18**, 25847 (2010).

[48] T. G. B. de Souza, E. C. Barbano, S. C. Zilio, and L. Misoguti, Measurement of nonlinear refractive indices of air, oxygen, and nitrogen in capillary by changing the temporal width of short laser pulses, J. Opt. Soc. Am. B **34**, 2233 (2017).

[49] F. Théberge, W. Liu, P. T. Simard, A. Becker, and S. L. Chin, Plasma density inside a femtosecond laser filament in air: Strong dependence on external focusing, Phys. Rev. E **74**, 036406 (2006).

[50] E. Yablonovitch and N. Bloembergen, Avalanche ionization and the limiting diameter of filaments induced by light pulses in transparent media, Phys. Rev. Lett. **29**, 907 (1972).

[51] A. Talebpour, J. Yang, and S. Chin, Semi-empirical model for the rate of tunnel ionization of N_2 and O_2 molecule in an intense Ti:sapphire laser pulse, Opt. Commun. **163**, 29 (1999).

[52] R. Lehe, M. Kirchen, I. A. Andriyash, B. B. Godfrey, and J. Vay, A spectral, quasi-cylindrical and dispersion-free particle-in-cell algorithm, Comput. Phys. Commun. **203**, 66 (2016).

[53] https://fbpic.github.io/index.html..

[54] https://openpmd-viewer.readthedocs.io/en/latest.

[55] M. V. Ammosov, N. B. Delone, and V. P. Krainov, Tunnel ionization of complex atoms and atomic ions in electromagnetic field, in *High Intensity Laser Processes*, edited by J. A. Alcock (International Society for Optics and Photonics SPIE, 1986), Vol. 664, pp. 138–141.

[56] M. Ferrario, D. Alesini, M. Anania, A. Bacci, M. Bellaveglia, O. Bogdanov, R. Boni, M. Castellano, E. Chiadroni, A. Cianchi, S. B. Dabagov, C. De Martinis, D. Di Giovenale, G. Di Pirro, U. Dosselli, A. Drago, A. Esposito, R. Faccini, A. Gallo, M. Gambaccini, *et al.*, SPARC_LAB present and future, Nucl. Instrum. Methods Phys. Res. Sect. B **309**, 183 (2013).

[57] R. Pompili, M. P. Anania, I. Balossino, M. Bellaveglia, A. Biagioni, F. Cardelli, M. Carillo, E. Chiadroni, A. Cianchi, G. Costa, L. Crincoli, A. Del Dotto, M. Del Franco, M. Del Giorno, R. Demitra, F. Demurtas, V. Dompè, A. Frazzitta, M. Galletti, A. Gallo, *et al.*, SPARC_LAB facility for advanced acceleration and radiation experiments, Phys. Rev. Accel. Beams **29**, 051602 (2026).

[58] D. Strickland and G. Mourou, Compression of amplified chirped optical pulses, Opt. Commun. **55**, 447 (1985).

[59] R. Pompili, E. Chiadroni, A. Cianchi, A. Curcio, A. Del Dotto, M. Ferrario, M. Galletti, S. Romeo, J. Scifo, V. Shpakov, F.

Villa, and A. Zigler, Time-resolved study of nonlinear photoemission in radio-frequency photoinjectors, Opt. Lett. **46**, 2844 (2021).

[60] L. Verra, M. Galletti, M. P. Anania, A. Biagioni, M. Carillo, E. Chiadroni, A. Cianchi, G. Costa, L. Crincoli, A. Del Dotto, M. Del Giorno, R. Demitra, G. Di Pirro, A. Giribono, V. Lollo, M. Opromolla, G. Parise, D. Pellegrini, R. Pompili, S. Romeo, *et al.*, Resonant excitation of plasma wakefields with a train of relativistic particle bunches, Phys. Rev. E **112**, 045205 (2025).

[61] L. Serafini and M. Ferrario, Velocity bunching in photoinjectors, AIP Conf. Proc. **581**, 87 (2001).

[62] M. Ferrario, D. Alesini, A. Bacci, M. Bellaveglia, R. Boni, M. Boscolo, M. Castellano, E. Chiadroni, A. Cianchi, L. Cultrera, G. Di Pirro, L. Ficcadenti, D. Filippetto, V. Fusco, A. Gallo, G. Gatti, L. Giannessi, M. Labat, B. Marchetti, C. Marrelli, *et al.*, Experimental demonstration of emittance compensation with velocity bunching, Phys. Rev. Lett. **104**, 054801 (2010).

[63] E. Arévalo and A. Becker, Theoretical analysis of fluorescence signals in filamentation of femtosecond laser pulses in nitrogen molecular gas, Phys. Rev. A **72**, 043807 (2005).

[64] D. Alesini, G. Di Pirro, L. Ficcadenti, A. Mostacci, L. Palumbo, J. Rosenzweig, and C. Vaccarezza, RF deflector design and measurements for the longitudinal and transverse phase space characterization at SPARC, Nucl. Instrum. Methods Phys. Res. Sect. A **568**, 488 (2006).

[65] R. D'Arcy, J. Chappell, J. Beinortaite, S. Diederichs, G. Boyle, B. Foster, M. J. Garland, P. Gonzalez Caminal, C. A. Lindstrøm, G. Loisch, S. Schreiber, S. Schröder, R. J. Shalloo, M. Thévenet, S. Wesch, M. Wing, and J. Osterhoff, Recovery time of a plasma-wakefield accelerator, Nature (London) **603**, 58 (2022).

[66] A. Biagioni, M. P. Anania, M. Bellaveglia, E. Chiadroni, A. Cianchi, D. Di Giovenale, G. Di Pirro, M. Ferrario, F. Filippi, A. Mostacci, R. Pompili, V. Shpakov, C. Vaccarezza, F. Villa, and A. Zigler, Electron density measurement in gas discharge plasmas by optical and acoustic methods, J. Instrum. **11**, C08003 (2016).

[67] M. Galletti, M. P. Anania, S. Arjmand, A. Biagioni, G. Costa, M. Del Giorno, M. Ferrario, V. Lollo, R. Pompili, Y. Raz, V. Shpakov, F. Villa, A. Zigler, and A. Cianchi, Advanced stabilization methods of plasma devices for plasma-based acceleration, Symmetry **14**, 450 (2022).

[68] E. Adli, A. Ahuja, O. Apsimon, R. Apsimon, A.-M. Bachmann, D. Barrientos, F. Batsch, J. Bauche, V. K. B. Olsen, M. Bernardini, T. Bohl, C. Bracco, F. Braunmüller, G. Burt, B. Buttenschön, A. Caldwell, M. Cascella, J. Chappell, E. Chevallay, M. Chung, *et al.*, Acceleration of electrons in the plasma wakefield of a proton bunch, Nature (London) **561**, 363 (2018).

[69] E. Gschwendtner, M. Turner, E. Adli, A. Ahuja, O. Apsimon, R. Apsimon, A.-M. Bachmann, F. Batsch, C. Bracco, F. Braunmüller, S. Burger, G. Burt, B. Buttenschön, A. Caldwell, J. Chappell, E. Chevallay, M. Chung, D. Cooke, H. Damerau, L. H. Deubner, *et al.*, Proton-driven plasma wakefield acceleration in AWAKE, Philos. Trans. R. Soc. A **377**, 20180418 (2019).

[70] R. W. Assmann, M. K. Weikum, T. Akhter, D. Alesini, A. S. Alexandrova, M. P. Anania, N. E. Andreev, I. Andriyash, M. Artioli, A. Aschikhin, T. Audet, A. Bacci, I. F. Barna, S. Bartocci, A. Bayramian, A. Beaton, A. Beck, M. Bellaveglia, A. Beluze, A. Bernhard, *et al.*, EuPRAXIA conceptual design report, Eur. Phys. J. Spec. Top. **229**, 3675 (2020).

[71] D. Alesini *et al.*, EuPRAXIA@SPARC_LAB technical design report, Technical Report (INFN, 2026).

[72] L. Crincoli, R. Demitra, V. Lollo, D. Pellegrini, M. Pitti, L. Pronti, M. Romani, M. Ferrario, and A. Biagioni, Advanced ceramic plasma discharge capillaries for high repetition rate operation, Sci. Rep. **15**, 12456 (2025).

[73] A. Biagioni, M. P. Anania, S. Arjmand, E. Behar, G. Costa, A. Del Dotto, M. Ferrario, M. Galletti, V. Lollo, D. Pellegrini, G. Di Pirro, R. Pompili, Y. Raz, G. Russo, and A. Zigler, Gas-filled capillary-discharge stabilization for plasma-based accelerators by means of a laser pulse, Plasma Phys. Control. Fusion **63**, 115013 (2021).

[74] D. H. Whittum, A. M. Sessler, and J. M. Dawson, Ion-channel laser, Phys. Rev. Lett. **64**, 2511 (1990).

[75] S. Diederichs, T. J. Mehrling, C. Benedetti, C. B. Schroeder, A. Knetsch, E. Esarey, and J. Osterhoff, Positron transport and acceleration in beam-driven plasma wakefield accelerators using plasma columns, Phys. Rev. Accel. Beams **22**, 081301 (2019).

[76] S. Gessner, J. Osterhoff, C. A. Lindstrøm, *et al.*, Design initiative for a 10 TeV pcm wakefield collider, arXiv:2503.20214.